ELectronics EXpress

LETTER

IEICE Electronics Express, Vol.11, No.12, 1–11

High-frequency uniform asymptotic solution for reflected and scattered fields over half-space metamaterial

Toru Kawano[1a)] **and Toyohiko Ishihara**[2]

[1] *Department of Communication Engineering, National Defense Academy, Hashirimizu 1–10–20, Yokosuka, Kanagawa 239–8686, Japan*

[2] *Retired from Department of Communication Engineering, National Defense Academy, Hashirimizu 1–10–20, Yokosuka, Kanagawa 239–8686, Japan*

a) *tkawano@nda.ac.jp*

Abstract: It is known that when the cylindrical wave propagates from a positive index material (PIM) to a negative index material (NIM), the backward lateral wave is excited along the interface between the PIM and the NIM over a half-space metamaterial. In this study, by using the saddle point technique, we shall derive a novel high-frequency uniform asymptotic solution for the reflected and scattered fields over a half-space metamaterial with the NIM. The validity and utility of the novel uniform asymptotic solution is confirmed by comparing with the reference solution calculated by the numerical integration of the integral representation for the reflected and scattered fields. We have also shown the physical interpretation of the uniform asymptotic solution.

Keywords: metamaterial, backward lateral wave, uniform asymptotic solution, reflected and scattered fields

Classification: Electromagnetic theory

References

[1] H. K. V. Lotsch: Optik **32** (1970) 116.

[2] B. R. Horowitz and T. Tamir: J. Opt. Soc. Am. **61** (1971) 586. DOI:10.1364/JOSA.61.000586

[3] J. W. Ra, H. L. Bertoni and L. B. Felsen: SIAM J. Appl. Math. **24** (1973) 396. DOI:10.1137/0124041

[4] S. Kozaki and H. Sakurai: J. Opt. Soc. Am. **68** (1978) 508. DOI:10.1364/JOSA.68.000508

[5] L. M. Brekhovskikh: *Waves in Layered Media* (Academic Press, New York, 1980) 2nd ed. chaps. 1 and 4.

[6] S. Zhang and C. Fan: J. Opt. Soc. Am. A **5** (1988) 1407. DOI:10.1364/JOSAA.5.001407

[7] L. B. Felsen and N. Marcuvitz, ed.: *Radiation and Scattering of Waves* (IEEE Press (Classic Reissue), New Jersey, 1994) sec. 5.5.

[8] T. Ishihara and Y. Miyagawa: IEICE Trans. Electron. **J82-C-I** (1999) 62.

[9] D. T. Quang, K. Goto, T. Kawano and T. Ishihara: IEICE Trans. Electron.

DOI: 10.1587/elex.11.20140284
Received March 28, 2014
Accepted April 15, 2014
Publicized June 9, 2014
Copyedited June 25, 2014

E95-C (2012) 16. DOI:10.1587/transele.E95.C.16
[10] V. G. Veselago: Sov. Phys. Usp. **10** (1968) 509. DOI:10.1070/PU1968v010n04ABEH003699
[11] P. M. Valanju, R. M. Walser and A. P. Valanju: Phys. Rev. Lett. **88** (2002) 187401. DOI:10.1103/PhysRevLett.88.187401
[12] D. R. Smith, D. Schurig and J. B. Pendry: Appl. Phys. Lett. **81** (2002) 2713. DOI:10.1063/1.1512828
[13] Z. M. Zhang and K. Park: Trans. of the ASME, J. Heat Transfer **126** (2004) 244. DOI:10.1115/1.1668035
[14] A. Ishimaru, J. R. Thomas and S. Jaruwatanadilok: IEEE Trans. Antenn. Propag. **53** (2005) 915. DOI:10.1109/TAP.2004.842572
[15] J. R. Thomas and A. Ishimaru: IEEE Tarns. Antenn. Propag. **53** (2005) 1591. DOI:10.1109/TAP.2005.846454
[16] T. Kawano and T. Ishihara: Proc. of ISAP2012, 2D1-1 (2012) 371.
[17] T. Kawano and T. Ishihara: The Papers of Technical Meeting on Electromagnetic Theory, IEE Japan, EMT-12-149 (2012) 167.
[18] S. A. Chin-Bing, J. A. Davis and R. B. Evans: J. Acoust. Soc. Am. **71** (1982) 1433. DOI:10.1121/1.387839
[19] L. B. Felsen and N. Marcuvitz, ed.: *Radiation and Scattering of Waves* (IEEE Press (Classic Reissue), New Jersey, 1994) chap. 4.
[20] E. T. Whittaker and G. N. Watson, ed.: *A Course of Modern Analysis* (Cambridge University Press, Cambridge, 1973) 347.

1 Introduction

It has been studied by many researchers that when a cylindrical wave, a spherical wave, or a Gaussian beam propagates from a denser medium to a rarer medium through the plane dielectric interface of the mediums, a totally reflected ray, a lateral wave, and an evanescent wave are excited and the Goos-Hänchen shift is generated [1, 2, 3, 4, 5, 6, 7, 8, 9]. The above mentioned researches have been treated the reflected and refracted electromagnetic fields for a plane dielectric interface composed of the mediums whose real parts of the permittivities, the permeabilities, and the refractive indices are all positive. While, Veselago has published a noteworthy paper on the transmission and the refraction of the electromagnetic wave through the metamaterial whose permittivity and permeability are simultaneously negative and thereby the refractive index is also negative [10].

After the publication of the paper by Veselago [10], many papers on the transmitted and refracted fields through the plane interface whose refractive index is negative have not been published for a long time. However, recently, many papers on the transmission and the refraction of the electromagnetic wave through the metamaterial interface and on a phase velocity, a group velocity, and a group-front velocity in the metamaterial have been published [11, 12, 13, 14, 15]. Especially, in [14], it has been shown that a backward lateral wave is excited along the plane boundary composed of an ordinary material and a metamaterial.

In this research, we shall derive a novel high-frequency uniform asymptotic solution for the reflected and scattered fields over a half-space meta-

DOI: 10.1587/elex.11.20140284
Received March 28, 2014
Accepted April 15, 2014
Publicized June 9, 2014
Copyedited June 25, 2014

material when a cylindrical wave emanated from a line source is incident on the plane metamaterial boundary from the ordinary material side, assuming that both the source and the observation points are placed in the ordinary material [9, 16, 17]. The novel uniform asymptotic solution derived in this paper is applicable in the transition region [9, 16, 17] near the geometrical boundary. The uniform asymptotic solution is composed of a geometrically reflected ray on the metamaterial plane, two kinds of backward lateral waves, and a transition wave which plays an important role in the transition region. We will clarify the validity and utility of the uniform asymptotic solution by comparing with the reference solution calculated from the numerical integration of the integral representation for the reflected and scattered fields over the half-space metamaterial. We will also clarify the physical interpretation of the uniform asymptotic solution.

2 Formulation and derivation of integral representation

Fig. 1 shows the Cartesian coordinate system (x, y, z), a plane interface defined by $z = 0$ consisting of an upper material (medium 1) and a lower material (medium 2), and the schematic figure of the reflected and scattered electromagnetic fields observed in the medium 1. A cylindrical wave emanated from a y-directed electric line source $\mathrm{Q}(x = 0, z = h)$ placed in the medium 1 is incident on the medium 2. The medium 1 is an ordinary material with a permittivity $\varepsilon_1(> 0)$ and a permeability $\mu_1(> 0)$ while the medium 2 is a metamaterial with a permittivity $\varepsilon_2(< 0)$ and a permeability $\mu_2(< 0)$. It is shown in Fig. 1 that the geometrically reflected ray $\mathrm{Q} \to \mathrm{A} \to \mathrm{P}(x, z)$ reflected at the point A on the medium 2 (the reflection angle is θ_0) and the backward lateral waves $\mathrm{Q} \to \mathrm{B} \to \mathrm{C} \to \mathrm{P}(x, z)$ and $\mathrm{Q} \to \mathrm{B}' \to \mathrm{C}' \to \mathrm{P}(x, z)$ are observed at the observation point $\mathrm{P}(x, z)$. In this paper, we will assume that the observation point $\mathrm{P}(x, z)$ is placed in the region satisfying $x > 0$ and $z > 0$. The notation $\mathrm{Q} \to \mathrm{A}$, for example, indicates the wave which propagates from the (source) point Q to the point A along the straight line QA (see

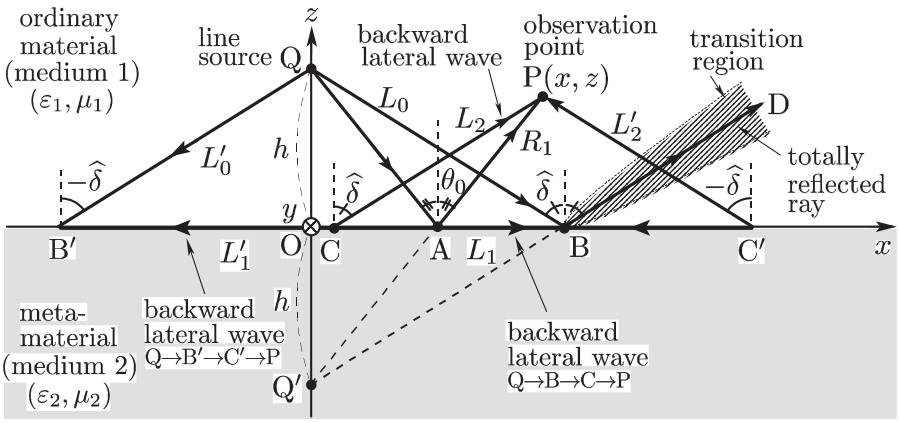

Fig. 1. Cartesian coordinate system (x, y, z) and scattering phenomena observed in the near region over half-space metamaterial. The shaded region denotes the transition region.

DOI: 10.1587/elex.11.20140284
Received March 28, 2014
Accepted April 15, 2014
Publicized June 9, 2014
Copyedited June 25, 2014

Fig. 1). The backward lateral waves are excited by the incident rays Q → B and Q → B′ whose incident angles are coincident with the critical angles $\widehat{\delta}$ and $-\widehat{\delta}$ of the total reflections, respectively.

In Fig. 1, the shaded area shows the transition region located near the geometrically reflected ray B → D with the reflection angle $\widehat{\delta}$. When the observation point P(x, z) is placed in the region farther than the transition region, the backward lateral wave Q → B → C → P depicted in Fig. 1 can not be observed. In this way, the reflection and scattering phenomena in the region nearer than the transition region are different from those in the region farther than the transition region.

The above mentioned reflected and scattered fields are described by the following integral representation [9, 14, 15, 16, 17].

$$E_y^r = \frac{i}{4\pi}\int_{-\infty}^{\infty} \Gamma(k_{1x})\frac{e^{ik_{1x}x+ik_{1z}(z+h)}}{k_{1z}}dk_{1x}, \tag{1}$$

$$\Gamma(k_{1x}) = \frac{k_{1z}/\mu_1 - k_{2z}/\mu_2}{k_{1z}/\mu_1 + k_{2z}/\mu_2}, \quad k_{1z} = \sqrt{k_1^2 - k_{1x}^2}, \quad k_{2z} = \sigma\sqrt{k_2^2 - k_{2x}^2}. \tag{2}$$

The time factor $\exp(-i\omega t)$ is suppressed throughout this paper. Note that the y-component of the electric field E_y^r is normalized as $i\omega\mu_1 J = 1$ (J: amplitude of electric current source). In (1) and (2), k_1 and $k_2(< 0)$ are the propagation constants in the mediums 1 and 2, k_{1x} and k_{2x} (k_{1z} and k_{2z}) are the x-components (the z-components) of k_1 and k_2, respectively. Since the medium 2 is the metamaterial, σ in (2) is defined as $\sigma = -1$.

The integrand of (1) possesses four branch points at $k_{1x} = \pm k_1, \pm|k_2|$ in the complex k_{1x}-plane. Therefore, in order to reduce the complexity of the analysis, one may transform the integral in (1) from the complex k_{1x}-plane to the complex θ-plane via $k_{1x} = k_1 \sin\theta$. Then the integral in (1) becomes as follows:

$$E_y^r = \frac{i}{4\pi}\int_{P_\theta} \Gamma(\theta)e^{ik_1R_1q(\theta)}d\theta, \tag{3}$$

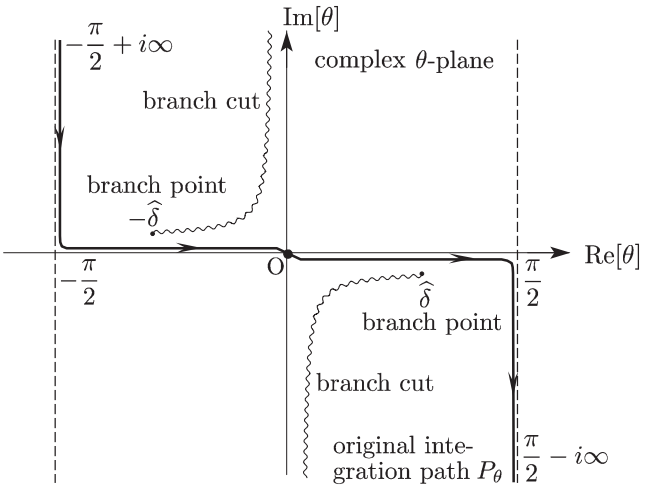

Fig. 2. Integration path P_θ and branch point singularities $\theta = \pm\widehat{\delta}$ associated with branch cuts in the complex θ-plane.

DOI: 10.1587/elex.11.20140284
Received March 28, 2014
Accepted April 15, 2014
Publicized June 9, 2014
Copyedited June 25, 2014

$$\Gamma(\theta) = \frac{\widehat{m}\cos\theta - \sqrt{\widehat{n}^2 - \sin^2\theta}}{\widehat{m}\cos\theta + \sqrt{\widehat{n}^2 - \sin^2\theta}},\ q(\theta) = \cos(\theta - \theta_0), \tag{4}$$

$$\widehat{m} = -m,\ m = \frac{\mu_2}{\mu_1},\ \widehat{n} = -n,\ n = -\frac{\sqrt{\varepsilon_2\mu_2}}{\sqrt{\varepsilon_1\mu_1}} < 0. \tag{5}$$

In the above equations, R_1 and θ_0 express, respectively, the propagation distance and the incident angle (or the reflection angle) of the geometrically reflected ray (see Fig. 1) and $q(\theta)$ is the phase function.

Fig. 2 shows the integration path and branch points $\theta = \pm\widehat{\delta}$ associated with branch cuts of the integral in the complex θ-plane defined by (3)$\sim$(5). The branch points are calculated from the condition that the function $\widehat{n}^2 - \sin^2\theta$ in the square root of (4) equals 0. Thus one may obtain the branch points $\theta = \pm\widehat{\delta}$ where $\widehat{\delta} = \sin^{-1}\widehat{n}$. The branch point $\theta = \widehat{\delta}$ corresponds physically to the critical angle $\widehat{\delta}$ of the totally reflected geometrical ray Q $\rightarrow$ B $\rightarrow$ D shown in Fig. 1.

3 Derivation of uniform asymptotic solution applicable in the transition region

3.1 Integral representations for geometrically reflected ray and scattered fields

It is difficult to analyze the integral in (3) because the function $\Gamma(\theta)$ in (3) is expressed by using the function $\widehat{n}^2 - \sin^2\theta$ in the square root (see (4)) [5, 7, 9, 16, 17, 18]. Therefore, in order to reduce the complexity of the asymptotic analysis, the function $\Gamma(\theta)$ corresponding to the reflection coefficient is decomposed into two portions, the terms which do not possess the branch point and the term which possesses the branch points, as follows [9, 16, 17, 18]:

$$\Gamma(\theta) = \Gamma(\theta_0) + \Gamma_s(\theta) + \Gamma^{(2)}(\theta)\sqrt{\sin(\widehat{\delta} - \theta)}\sqrt{\sin(\widehat{\delta} + \theta)}, \tag{6}$$

where $\Gamma_s(\theta)$ and $\Gamma^{(2)}(\theta)$ are defined by

$$\Gamma_s(\theta) = \Gamma^{(1)}(\theta) - \Gamma^{(1)}(\theta_0) - \Gamma^{(2)}(\theta_0)\sqrt{\sin(\widehat{\delta} - \theta_0)}\sqrt{\sin(\widehat{\delta} + \theta_0)}, \tag{7}$$

$$\Gamma^{(1)}(\theta) = \frac{\widehat{m}^2\cos^2\theta - (\sin^2\theta - \widehat{n}^2)}{\widehat{m}^2\cos^2\theta + \sin^2\theta - \widehat{n}^2}, \tag{8}$$

$$\Gamma^{(2)}(\theta) = \frac{-2\widehat{m}\cos\theta}{\widehat{m}^2\cos^2\theta + \sin^2\theta - \widehat{n}^2}. \tag{9}$$

By substituting (6) into (3), the electric field E_y^r is expressed by the integrals corresponding to the geometrically reflected ray E_y^{go} and the scattered fields E_y^s.

$$E_y^r = E_y^{go} + E_y^s, \tag{10}$$

$$E_y^{go} = \frac{i}{4\pi}\Gamma(\theta_0)\int_{P_\theta} e^{ik_1R_1q(\theta)}d\theta, \tag{11}$$

$$E_y^s = E_y^{s1} + E_y^{s2}, \tag{12}$$

$$E_y^{s1} = \frac{i}{4\pi}\int_{P_\theta} \Gamma_s(\theta)e^{ik_1R_1q(\theta)}d\theta, \tag{13}$$

$$E_y^{s2} = \frac{i}{4\pi}\int_{P_\theta} \Gamma^{(2)}(\theta)\sqrt{\sin(\widehat{\delta} - \theta)}\sqrt{\sin(\widehat{\delta} + \theta)}\ e^{ik_1R_1q(\theta)}d\theta. \tag{14}$$

DOI: 10.1587/elex.11.20140284
Received March 28, 2014
Accepted April 15, 2014
Publicized June 9, 2014
Copyedited June 25, 2014

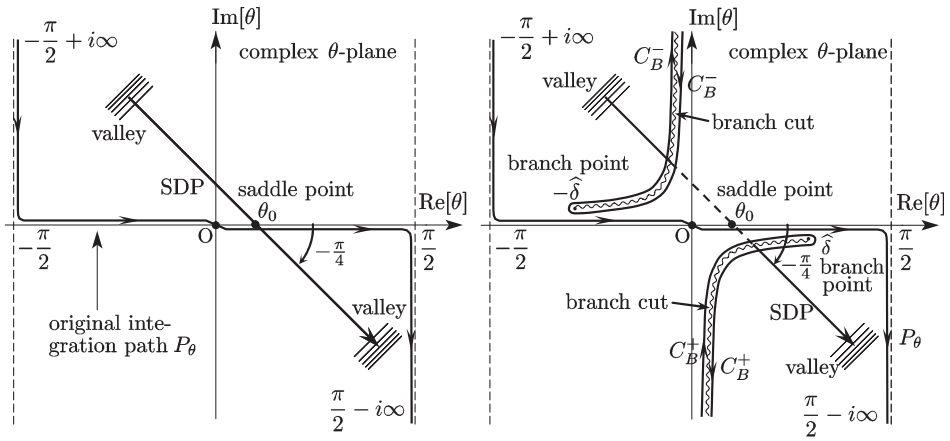

(a) Original integration path P_θ and steepest descent path (SDP) through saddle point $\theta = \theta_s = \theta_0$.

(b) Branch points $\theta = \pm\widehat{\delta}$ with branch cuts and SDP passing through saddle point at $\theta = \theta_s = \theta_0$.

Fig. 3. Steepest descent path and branch points associated with branch cuts in the complex θ-plane.

3.2 Asymptotic solution for geometrically reflected ray

The integrand of the geometrically reflected ray E_y^{go} in (11) does not possess any singular point in the complex θ-plane. Therefore, if the high-frequency condition $k_1 R_1 \gg 1$ is satisfied, as shown in Fig. 3(a), the original integration path P_θ is deformed into the SDP (Steepest Descent Path) passing through the saddle point $\theta = \theta_s = \theta_0$ defined by the saddle point equation $(d/d\theta)q(\theta) = -\sin(\theta - \theta_0) = 0$ (see (4)) [19]. Then by applying the isolated saddle point technique [19], one may obtain the first-order asymptotic solution for E_y^{go} as follows:

$$E_y^{go} \sim \frac{i}{4}\sqrt{\frac{2}{\pi k_1 R_1}}\, e^{ik_1 R_1 - i\pi/4}\Gamma(\theta_0). \tag{15}$$

The asymptotic solution E_y^{go} in (15) is identified as the geometrical ray $\mathrm{Q} \to \mathrm{A} \to \mathrm{P}(x, z)$ which is reflected with the reflection coefficient $\Gamma(\theta_0)$ at the point A on the metamaterial and reaches the observation point $\mathrm{P}(x, z)$ (see Fig. 1). It is shown in Fig. 1 that the saddle point $\theta = \theta_s = \theta_0$ of the integrand in the complex θ-plane corresponds to the incident angle (or the reflection angle) of the geometrically reflected ray.

3.3 Asymptotic solutions for scattered fields applicable in transition region

In (13), the integrand of E_y^{s1}, which is a portion of the scattered field E_y^s in (10) and (12), does not possess any singular point in the complex θ-plane. Therefore, the asymptotic analysis method for E_y^{s1} is similar to the one for E_y^{go} corresponding to the geometrically reflected ray. Thus deforming the original integration path P_θ into the SDP (see Fig. 3(a)) and applying the isolated saddle point technique [19], one may obtain the following first-order asymptotic solution:

$$E_y^{s1} \sim -\Gamma^{(2)}(\theta_0)\sqrt{\sin(\widehat{\delta} - \theta_0)}\sqrt{\sin(\widehat{\delta} + \theta_0)}\,\frac{i}{4}\sqrt{\frac{2}{\pi k_1 R_1}}\, e^{ik_1 R_1 - i\pi/4}. \tag{16}$$

DOI: 10.1587/elex.11.20140284
Received March 28, 2014
Accepted April 15, 2014
Publicized June 9, 2014
Copyedited June 25, 2014

It is remained to derive the asymptotic solution for the scattered field E_y^{s2} defined in (14). The integrand of E_y^{s2} in (14) possesses the branch points at $\theta = \pm\widehat{\delta}$ in addition to the saddle point at $\theta = \theta_s = \theta_0$. The branch points at $\theta = \pm\widehat{\delta}$ associated with the branch cuts of the integrand in (14) are shown in Fig. 3(b) [5, 7, 8, 14, 17]. The steepest descent path (SDP) passing through the saddle point $\theta = \theta_s = \theta_0$ obtained from the saddle point equation $dq(\theta)/d\theta = 0$ is also shown in Fig. 3(b).

By deforming the original integration path P_θ for the integral E_y^{s2} into the SDP passing through the saddle point $\theta = \theta_0$ as shown in Fig. 3(b), two branch cuts are traversed by the SDP when the saddle point θ_0 is located in the region satisfying $0 < \theta_0 \leq \widehat{\delta}$. As seen from Fig. 1, the region $0 < \theta_0 \leq \widehat{\delta}$ corresponds physically to the case when the observation point P is placed in the region closer than the geometrical boundary shown by the solid line BD. Therefore, when the observation point P is placed in the region closer than the geometrical boundary BD, the contribution to the integral E_y^{s2} in (14) may arise from the integration paths along C_B^- and C_B^+ around the branch cuts for the branch points $-\widehat{\delta}$ and $\widehat{\delta}$, respectively, in addition to the SDP as shown in Fig. 3(b) [5, 7, 8, 9, 14, 16, 17, 18]. Thus one may represent E_y^{s2} in (14) by

$$E_y^{s2} = E_y(-\widehat{\delta}) + E_y(\widehat{\delta}) + E_y(\mathrm{SDP}), \quad 0 < \theta_0 \leq \widehat{\delta}, \tag{17a}$$

where $E_y(-\widehat{\delta})$, $E_y(\widehat{\delta})$, and $E_y(\mathrm{SDP})$ denote, respectively, the asymptotic solutions obtained from the integration paths C_B^-, C_B^+, and the SDP. While when the observation point P is placed in the region fartherthan the solid line BD, the contribution to the integral E_y^{s2} may arise from the integration paths along C_B^- around the branch cut associated with the branch point $-\widehat{\delta}$ and along the SDP [5, 7, 8, 9, 14, 16, 17, 18]. In this case, E_y^{s2} may be expressed as

$$E_y^{s2} = E_y(-\widehat{\delta}) + E_y(\mathrm{SDP}), \quad \widehat{\delta} < \theta_0 < \frac{\pi}{2}. \tag{17b}$$

Thus by combining (17a) and (17b), the integral E_y^{s2} in (14) may be represented by

$$E_y^{s2} = E_y(-\widehat{\delta}) + U(\widehat{\delta} - \theta_0)E_y(\widehat{\delta}) + E_y(\mathrm{SDP}), \tag{18}$$

where $U(\widehat{\delta} - \theta_0)$ is the unit step function defined by $U(x) = 1$ for $x \geq 0$ and $U(x) = 0$ for $x < 0$. Note that we have assumed that θ_0 is located in the range $0 < \theta_0 < \pi/2$ (see Fig. 1).

The asymptotic analysis methods for the integration around the branch cut associated with the branch point singularity have been studied in the references [5, 7, 8, 9, 16, 18]. Therefore, extending the procedures given in [5, 7, 8, 9, 16, 18] and assuming that the branch point $\theta = -\widehat{\delta}$ is located far away from the saddle point $\theta = \theta_0$ and the branch point $\theta = \widehat{\delta}$ is located close to the saddle point $\theta = \theta_0$, one may obtain, after cumbersome but straightforward analyses, the asymptotic solutions for $E_y(-\widehat{\delta})$ and $E_y(\widehat{\delta})$ in (18) as follows:

$$E_y(-\widehat{\delta}) \sim \frac{\sqrt{n}\exp(i\pi/4)}{\sqrt{2\pi}\widehat{m}k_1^{3/2}(1-\widehat{n}^2){L_1'}^{3/2}} e^{ik_1(L_0'+L_2')-i\widehat{k}_2 L_1'}, \tag{19}$$

DOI: 10.1587/elex.11.20140284
Received March 28, 2014
Accepted April 15, 2014
Publicized June 9, 2014
Copyedited June 25, 2014

$$E_y(\widehat{\delta}) \sim \frac{\sqrt{n}\exp(i\pi/4)}{\sqrt{2\pi}\widehat{m}k_1^{3/2}(1-\widehat{n}^2){L_1}^{3/2}} e^{ik_1(L_0+L_2)-i\widehat{k_2}L_1} \cdot \left[\frac{D_{-3/2}(\xi+i\xi)}{2^{-3/4}\xi^{-3/2}\exp(-i3\pi/8)\exp(-i\xi^2/2)}\right],$$

$$k_2 = -\widehat{k_2}, \quad \widehat{k_2} = \omega\sqrt{\varepsilon_2\mu_2} > 0, \tag{20}$$

$$\xi = \sqrt{2k_1R_1}\sin\frac{\widehat{\delta}-\theta_0}{2}, \tag{21}$$

where $D_\nu(z)$ used in (20) denotes the parabolic cylinder function [20]. The notations $L_0'(=\mathrm{QB}')$, $L_1'(=\mathrm{B}'\mathrm{C}')$, and $L_2'(=\mathrm{C}'\mathrm{P})$ and $L_0(=\mathrm{QB})$, $L_1(=\mathrm{BC})$, and $L_2(=\mathrm{CP})$ used in (19) and (20) are defined in Fig. 1.

The geometrical path of the asymptotic solution $E_y(-\widehat{\delta})$ in (19) has been shown in Fig. 1. The electromagnetic wave emanated from the electric line source Q is incident on the plane metamaterial (medium 2) at the point B′ with the incident angle $-\widehat{\delta}$. Then the phase of $E_y(-\widehat{\delta})$ progresses to the backward direction from the point C′ to the point B′ [14]. The backward lateral wave $E_y(-\widehat{\delta})$ scattered at the point C′ with the critical angle $-\widehat{\delta}$ reaches the observation point $\mathrm{P}(x,z)$. In Fig. 1, by using similar manner, we have also shown the propagation trajectory of the asymptotic solution $E_y(\widehat{\delta})$ in (20). The electromagnetic wave emanated from the source Q is incident on the metamaterial at the point B with the incident angle $\widehat{\delta}$. Then the phase of the backward lateral wave $E_y(\widehat{\delta})$ progresses to the backward direction from C to B [14]. The backward lateral wave $E_y(\widehat{\delta})$ is scattered at the point C with the scattering angle $\widehat{\delta}$ coincident with the critical angle of the total reflection and reaches the observation point $\mathrm{P}(x,z)$ (see (20) and Fig. 1). As described above, the physical interpretations of the asymptotic solutions $E_y(-\widehat{\delta})$ and $E_y(\widehat{\delta})$ are clarified by drawing the propagation trajectories using the asymptotic solutions.

While the integral $E_y(\mathrm{SDP})$ in (18) along the SDP may be evaluated asymptotically by assuming that the saddle point θ_0 is located near the branch point $\widehat{\delta}$. The analysis methods for the integration along the SDP in the case when the saddle point is located near the branch point have been investigated in [5, 7, 8, 9, 16, 18]. Thus, applying the analysis methods given in the references [5, 7, 8, 9, 16, 18] and performing lengthy but straightforward calculations, the asymptotic solution for the integral along the SDP in Fig. 3(b) is obtained as follows:

$$E_y(\mathrm{SDP}) \sim \Gamma^{(2)}(\delta)\sqrt{\sin(\widehat{\delta}-\theta_0)}\sqrt{\sin(\widehat{\delta}+\theta_0)}\,\frac{i}{4}\sqrt{\frac{2}{\pi k_1R_1}} \cdot e^{ik_1R_1-i\pi/4}\frac{D_{1/2}(|\xi|-i|\xi|)}{2^{1/4}|\xi|^{1/2}\exp(-i\pi/8)\exp(i|\xi|^2/2)}. \tag{22}$$

By substituting the asymptotic solutions E_y^{s1} in (16) and E_y^{s2} in (18) into (12), one may obtain the asymptotic solution for the scattered field E_y^s as follows:

$$E_y^s = E_y(-\widehat{\delta}) + U(\widehat{\delta}-\theta_0)E_y(\widehat{\delta}) + E_y^{tran}, \tag{23}$$

where E_y^{tran} denotes the newly derived transition wave which plays an important role only in the transition region near the geometrical boundary BD traversed by the totally reflected ray (see Fig. 1) and is expressed as

DOI: 10.1587/elex.11.20140284
Received March 28, 2014
Accepted April 15, 2014
Publicized June 9, 2014
Copyedited June 25, 2014

$$E_y^{tran} = E_y^{s1} + E_y(\mathrm{SDP})$$
$$\sim \Gamma^{(2)}(\widehat{\delta})\sqrt{\sin(\widehat{\delta}-\theta_0)}\sqrt{\sin(\widehat{\delta}+\theta_0)}\,\frac{i}{4}\sqrt{\frac{2}{\pi k_1 R_1}}\,e^{ik_1R_1-i\frac{\pi}{4}}$$
$$\cdot\left[\frac{D_{1/2}(|\xi|-i|\xi|)}{2^{1/4}|\xi|^{1/2}\exp(-i\pi/8)\exp(i|\xi|^2/2)}-1\right]. \tag{24}$$

When the observation point $P(x,z)$ is located far away from the transition region (see Fig. 1), $|\xi|$ defined in (21) takes the large values i.e., $|\xi| \gg 1$. Then the parabolic cylinder function $D_{1/2}(|\xi|-i|\xi|)$ is approximated by [9, 20]

$$D_{1/2}(x-ix) \sim 2^{1/4}x^{1/2}e^{-i\pi/8}e^{ix^2/2}, \quad x \gg 1. \tag{25}$$

Therefore, the terms inside the parentheses [ ] in (24) approach zero as the value $|\xi|$ increases.

In the section 4, we will clarify that the transition wave E_y^{tran} in (24) contributes to the scattered fields E_y^s significantly (see (23)) only in the transition region and approaches zero outside the transition region.

3.4 Uniform asymptotic solution applicable in transition region

In the previous section, we have derived two kinds of the backward lateral waves and the transition wave which plays an important role in the transition region. By substituting (23) into (10), one may obtain the novel high-frequency uniform asymptotic solution consisting of the geometrically reflected ray E_y^{go}, the backward lateral waves $E_y(-\widehat{\delta})$ and $E_y(\widehat{\delta})$, and the transition wave E_y^{tran} as follows:

$$E_y^r = E_y^{go} + E_y(-\widehat{\delta}) + U(\widehat{\delta}-\theta_0)E_y(\widehat{\delta}) + E_y^{tran}. \tag{26}$$

The geometrical picture for the uniform asymptotic solution in (26) has been shown in Fig. 1. In the following section, we will clarify the validity of the uniform asymptotic solution in (26).

4 Numerical results and discussions

We have performed extensive numerical calculations. However, we will show here only the typical examples since all results are similar to those shown here if the numerical values used in the calculations satisfy the high-frequency condition.

In Fig. 4(a), the geometrically reflected ray (see (15)) constructing the uniform asymptotic solution in (26) is shown by the dotted curve (- - -). Also, the backward lateral waves $E_y(-\widehat{\delta})$ (see (19)) and $E_y(\widehat{\delta})$ (see (20)) and the transition wave E_y^{tran} in (24) are shown by the thick dashed curve (**– –**) and the dashed curve (– –) and the chain-dotted curve (– · –), respectively. Numerical values used in the calculations are shown in the figure.

The field amplitudes are calculated as a function of the incident angle θ_0; the observation point P(x,z) moves along the x-direction by keeping the height at $z = 80\lambda$ (see Fig. 1). Note that we have normalized the scattered field amplitudes by $(1/4)\sqrt{2/(\pi k_1 R_1)}$. In this example, the critical angle $\widehat{\delta}$ of the total reflection is 55° ($\varepsilon_1 = 2\varepsilon_0, |\varepsilon_2| \simeq 1.342\varepsilon_0$) (see Fig. 1). It is revealed

DOI: 10.1587/elex.11.20140284
Received March 28, 2014
Accepted April 15, 2014
Publicized June 9, 2014
Copyedited June 25, 2014

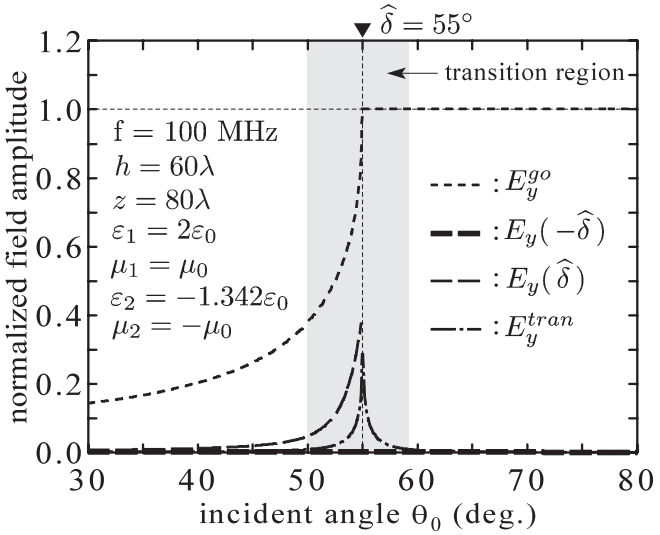

(a) Asymptotic solutions constructing uniform asymptotic solution.

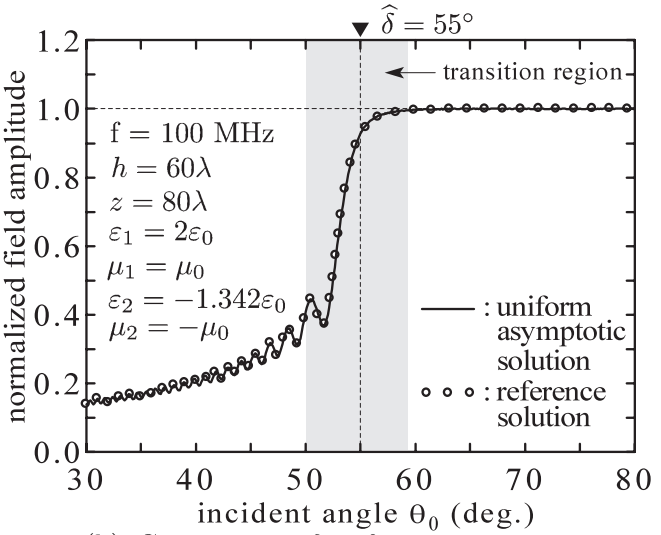

(b) Comparison of uniform asymptotic solution with reference solution.

Fig. 4. Comparisons between uniform asymptotic solution and reference solution. Various values used in calculations are given in the figures.

that, as θ_0 approaches the critical angle $\widehat{\delta}$, the amplitude of the geometrically reflected ray $|E_y^{go}|$ increases monotonically up to 1, and $|E_y^{go}|$ takes the constant value 1 in the region where θ_0 is greater than $\widehat{\delta}$. While, the backward lateral wave $E_y(-\widehat{\delta})$ becomes very small value as θ_0 increases. This is due to the fact that the propagation distance L_1' from the point B′ to the point C′, where the phase of $E_y(-\widehat{\delta})$ progresses to the backward direction from C′ to B′, takes the large value (see Fig. 1) and the amplitude of the backward lateral wave $E_y(-\widehat{\delta})$ decreases according to $(1/L_1')^{3/2}$ (see (19)). While the other type of the backward lateral wave $E_y(\widehat{\delta})$ $(--)$ increases monotonically in the region satisfying $0° < \theta_0 \leq 55°$ as θ_0 approaches the critical angle $\widehat{\delta} = 55°$.

Furthermore, the transition wave E_y^{tran} $(-\cdot-)$ increases in the region $0 < \theta_0 \leq 55°$ and becomes the maximum amplitude at the critical angle

DOI: 10.1587/elex.11.20140284
Received March 28, 2014
Accepted April 15, 2014
Publicized June 9, 2014
Copyedited June 25, 2014

$\theta_0 = \widehat{\delta} = 55°$. E_y^{tran} decreases monotonically in the region $\theta_0 > 55°$ as the observation point moves away from the critical angle $\widehat{\delta} = 55°$. It is clear that the transition wave plays the important role in the transition region near the critical angle $\widehat{\delta} = 55°$ shown by the shade in Fig. 1.

In Fig. 4(b), we have compared the uniform asymptotic solution in (26) obtained by using the calculation results in Fig. 4(a) with the reference solution obtained by performing the numerical integration of the integral (3). It is clarified that the uniform asymptotic solution (—) agrees very well with the reference solution (∘∘∘). Thus, the validity of the uniform asymptotic solution in (26) and the asymptotic solutions in (15), (19), (20), and (24) constructing the uniform asymptotic solution is confirmed.

5 Conclusion

In this study, we have investigated the electromagnetic fields over the half-space metamaterial when a cylindrical wave emanated from the line source located in the ordinary material is incident on the metamaterial. We have derived the novel high-frequency uniform asymptotic solution for the reflected and scattered fields over a half-space metamaterial with a negative index material. By comparing with the reference solution obtained from the numerical integration of the integral representation for the reflected and scattered fields, we have confirmed the validity of the uniform asymptotic solution. Furthermore, we have clarified the physical interpretation of the uniform asymptotic solution.

DOI: 10.1587/elex.11.20140284
Received March 28, 2014
Accepted April 15, 2014
Publicized June 9, 2014
Copyedited June 25, 2014